The Influence of the Compatible Solute Ectoine on the Local Water Structure: Implications for the Binding of the Protein G5P to DNA

Marc Benjamin Hahn,[†,§] Tihomir Solomun,[*,†] Robert Wellhausen,[‡] Sabrina Hermann,[‡] Harald Seitz,[‡] Susann Meyer,[†] Hans-Jörg Kunte,[†] Johannes Zeman,[¶] Frank Uhlig,[¶] Jens Smiatek,[*,¶] and Heinz Sturm[†,‖]

Federal Institute for Materials Research and Testing, D-12205 Berlin, Germany, Fraunhofer Institute for Cell Therapy and Immunology, D-14476 Potsdam-Golm, Germany, and Institute for Computational Physics, University of Stuttgart, D-70569 Stuttgart, Germany

E-mail: tihomir.solomun@bam.de; smiatek@icp.uni-stuttgart.de

Abstract

In order to survive extreme environmental conditions, microorganisms accumulate molar concentrations of compatible solutes which, among other effects prevent proteins from denaturation. A prominent example for a compatible solute is ectoine. Direct structural or spectroscopic information on the mechanism of the protein structure protection effect and the hydration shell around ectoine is scarce. In this work, surface

[*]To whom correspondence should be addressed
[†]Federal Institute for Materials Research and Testing, D-12205 Berlin, Germany
[‡]Fraunhofer Institute for Cell Therapy and Immunology, D-14476 Potsdam-Golm, Germany
[¶]Institute for Computational Physics, University of Stuttgart, D-70569 Stuttgart, Germany
[§]Free University Berlin, Department of Physics, D-14195 Berlin, Germany
[‖]Technical University Berlin, D-10587 Berlin, Germany

plasmon resonance (SPR), confocal Raman spectroscopy and molecular dynamics simulations were applied to study the local hydration shell of the zwitterionic osmolyte ectoine and its influence on the binding of a gene-5-protein (G5P) to a single-stranded DNA (dT_{25}). Due to the very high hygroscopicity of ectoine, it was possible to analyse its highly stable hydration shell by confocal Raman spectroscopy. Corresponding molecular dynamics simulation results revealed a significant change of the water dielectric constant in presence of a high molar ectoine concentration as compared to pure water. The SPR data showed that ectoine also has a derogatory influence on the amount of bound protein to DNA and on the protein-DNA dissociation rate constant in a concentration-dependent manner. Concomitantly, the Raman spectra in terms of the amide I region revealed large changes in the protein secondary structure. Our results indicate that ectoine strongly affects the molecular recognition between the protein and the oligonucleotide, which has important consequences for osmotic regulation mechanisms.

Introduction

Compatible solutes, also called osmolytes or co-solutes, such as ectoine among others, are synthesized by extremophilic microorganisms in order to maintain an osmotic equilibrium with the surrounding medium under conditions of extreme environmental salinity or thermal and pressure stresses[1,2]. Most compatible solutes are built of amino acids, polyols, sugars and heteroside derivatives[3–7]. Interestingly, compatible solutes do not disturb the cell's metabolism, even at high cytoplasmic concentrations. Many of these molecules stabilize macromolecules and cells, and have applications in biotechnology, agriculture, and medicine[8,9].

One of the beneficial mechanisms of compatible solutes is the stabilization of proteins which has attracted a lot of scientific attention[6,10–13]. Nevertheless, structural insight into this beneficial effect is still missing and the underlying mechanism is under debate. Most of the

suggested mechanisms propose an indirect interaction whereby a compatible solute does not directly interact with the solute. An important theory related to this assumption is given by the preferential exclusion model, which states that the co-solute is repelled into the bulk, in turn excess water molecules accumulate at the surface of the macromolecules, resulting in a preferential hydration of the protein[11]. Therefore, the unfolding of the protein becomes less favorable and the native form is conserved[1,11].

Indeed, in addition to protein structure protectants like ectoine, hydroxyectoine or TMAO (trimethylamine N-oxide), which are also water structure stabilizers (kosmotropes), some small molecules like urea or guanidinium are known as protein structure denaturants which weaken the water structure (chaotropes)[14–16]. Thus, a direct connection between chaotropes and kosmotropes on the one hand and protein structure denaturants and protein structure protectants on the other hand can be drawn[6,7]. A well-established framework to qualitatively discuss the underlying mechanisms for denaturants and protectants was introduced by the law of matching water affinities[14–16]. In this context, it was proposed that denaturants directly interact with protein surfaces whereas protectants are located in the second and third hydration shell. Thus, one can either observe a preferential binding mechanism for denaturants or a preferential exclusion mechanism for protectants in agreement to the preferential hydration model[10,11]. Indeed, this description has been often revealed as being too general. In a recent publication[17], it has been demonstrated that also the chemical properties of the major solute impose a significant contribution to the resulting preferential binding or preferential exclusion behavior. Hence, an a priori definition of chaotropic or kosmotropic properties is questionable. The validity of this observation has also been verified for complex co-solutes like ionic liquids that show a more subtle binding and exclusion mechanism[18].

In terms of ectoine, numerical and experimental results clearly indicated hygroscopic and kosmotropic properties[19] and a preferential exclusion mechanism around antifreeze peptides[20] and DPPC lipid bilayers[21,22]. Although a large number of studies focused on co-solutes and protein interactions, the effect of compatible solutes on oligonucleotides has been only

sparsely analyzed[23]. Present attempts mostly focus on technological aspects such as an enhancement of PCR reaction rates[24].

In the present study, we use surface plasmon resonance (SPR), confocal Raman spectroscopy, and density functional theory (DFT) in combination with molecular dynamics simulations to analyze in detail the influence of ectoine on the local water shell, the secondary structure of the protein G5P and on the binding of a single-strand binding protein (G5P) to immobilized dT_{25} oligonucleotides at a high DNA surface coverage, which mimics the situation in cells, where the concentration of biomolecules is high.

The manuscript is organized as follows. First, the experimental and computational details are presented in section 2. In section 3, we focus on ectoine molecules and their influence on the local water shell. Hereafter, we show surface plasmon resonance (SPR) data validating the influence of ectoine on the binding behavior of gene-5-proteins (G5P) to immobilized single-stranded DNA. Finally, we present Raman spectroscopy data from the amide I region of G5P indicating the influence of ectoine on the secondary structure elements of the protein. We briefly summarize and discuss the observed effects and the corresponding implications in section 4.

Experimental and computational details

Materials

Ectoine with a purity higher than 99% was obtained from Bitop (Witten, Germany). HPLC purified thiol-modified oligonucleotides (5′-HS-C_6-dT_{25}-3′) were obtained from Thermo Fischer Scientific (Ulm, Germany). Water for chromatography and D_2O (99.96% for NMR) were obtained from Merck (Darmstadt, Germany). SPR gold-on-glass chips were obtained from GE HealthCare (Munich, Germany). The protein G5P (Swissprot: P69544, 87 AA, Mw 9688 Da) from bacteriophage M13 was expressed and purified as described in a recent publication[25]. In agreement with a previous publication[26], the G5P plasmid PET-30b was

transformed into BL21:DE3 and grown on a 2YT agar plate with 50 μg/ml kanamycin (2 ml overnight culture was inoculated into 200 ml 2YT medium with 50 μg/ml kanamycin). The protein was expressed with 1 mM IPTG at OD600 = 0.5 for 3 h. Cells were collected, resuspended in a 5 ml buffer solution (1×PBS, 10 mM imidazol) and sonicated. Cell debris was removed and the supernatant purified with 0.75 ml Ni-NTA agarose (Qiagen, Hilden, Germany). Resin was washed three times with 5 ml buffer solution (1×PBS, 20mM imidazole) and the protein was eluded with 5.1 ml buffer solution (1×PBS, 250 mM imidazole). Eluate was concentrated with Amicon, 0.2 μm pore size, in ultra centrifugal devices (Merck Chemicals, Schwalbach, Germany) and the buffer was changed to 1×PBS using NAP-25 columns (GE-Healthcare, Munich, Germany). The protein concentration was determined with a BC-assay. For the Raman measurements, the protein was lyophilized from 1×PBS buffer to obtain a protein concentration of 12.6 mg/ml (2×PBS).

Experimental Methods

Preparation and confocal Raman spectra measurements

The dT_{25} layer was formed by immersing gold chips for 120 mins in a 10 μM solution of the oligonucleotides in 2×SSC followed by washing. Based on previous studies[27], the surface coverage of dT_{25} was estimated with $\sigma \sim 5 \times 10^{12}$ molecules/cm^2. The SPR experiments were carried out at a flow rate of 10 μl/min using a Biacore T-100 instrument (Uppsala, Sweden). The Raman spectra were obtained with a confocal Alpha300R instrument (WITec, Ulm, Germany) with 488 nm excitation wavelength and 25 mW laserpower. The laser light was focused on a drop (15 μl) of solution on high precision glass slide in high humidity atmosphere. Ten spectra with 60 s accumulation time were averaged. Dry ectoine powder was placed in a closed precision cuvette together with a separated drop of water nearby. The laser light was focused onto the small amount of dry powder and the spectra were collected continuously and averaged over a time interval of 10 s. In fact, the humidity within the cuvette increased rapidly to a saturation value such that the hydration of ectoine was initiated.

Surface plasmon resonance experiments and curve-fitting of the Amide I region for Raman spectra

Surface plasmon resonance is a method allowing biomolecular interactions to be monitored in real time under conditions of continuous flow over a sensor chip surface. The change in resonance angle (expressed in resonance units, RU) is proportional to the surface concentration (mass per unit area) of adsorbed molecules. With regard to the binding of the gene-5-protein to immobilized DNA strands, an experimental study[28] established a conversion factor of 1.3 RU per 10^{-10} g/cm^2 for biomolecules directly attached to a gold surface without a covering dextran layer.

Raman spectroscopy is one of the most commonly used methods[29–32] to extract information about the secondary structure of proteins by analysis of the amide I band envelope at 1600-1700 cm^{-1}. The amide I mode includes a carbonyl C=O stretching, with a small contribution from C-N stretching and N-H bending mode. The Raman signature of the amide group is extraordinarily sensitive to the polypeptide backbone conformation and provides direct quantitative information about the secondary structure of proteins. Prior to a curve-fitting procedure for the amide I region, the Raman spectra were treated as follows: i) the spectra were smoothed by Savitzky-Golay algorithm; ii) the spectra were normalized using the 1002 cm^{-1} line of phenylalanine, iii) the buffer/background spectrum was subtracted; iv) the ectoine contribution was subtracted by using its characteristic band at 1141 cm^{-1}; v) a zero-base line was drawn from 1530 to 1700 cm^{-1}, vi) the region between 1625 and 1700 cm^{-1} was normalized so that the sum of the intensity equals one. The actual curve-fitting procedure was carried out using multiple linear regression and Gauss-Lorentz profiles provided by the program OMNIC (ThermoElectron Corp.). Two bands at about 1604 cm^{-1} and 1612 cm^{-1}, stemming from ring modes of aromatic side chains were included in the amide I bands during the curve fitting procedure since they were not baseline-separated from the amide I feature.

Theoretical Methods

Atomistic Molecular Dynamics simulations and DFT calculations

All molecular dynamics simulations were performed with the software package GROMACS 4.5.5[33,34]. We considered zwitterionic ectoine molecules (Fig. 1) employing the force field presented in Ref. 19 in combination with the SPC/E water model[35].

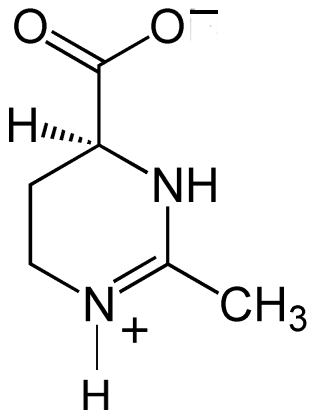

Figure 1: Chemical structure of zwitterionic ectoine.

The system was simulated in a cubic simulation box with periodic boundary conditions and initial dimensions of $(2.36 \times 2.36 \times 2.36)$ nm^3 in which 341 water and 12 ectoine molecules were inserted which corresponds to a molar ectoine concentration of $c = 1.64$ mol/L. Electrostatic interactions have been calculated by the Particle Mesh Ewald method[36]. The time step was $\Delta t = 1$ fs and the temperature was kept constant by a Nose-Hoover thermostat[37] choosing a temperature of 300 K with a thermostat relaxation time of 0.5 ps. Furthermore we used the Parrinello-Rahman barostat[38] with a relaxation time of 1 ps to adjust a constant pressure of 1 bar. All bonds have been constrained by the LINCS algorithm[39]. After energy minimization, we conducted a constant pressure and constant temperature NpT equilibration run of 5 ns and a NpT production run of 100 ns.

Furthermore we conducted a simulation run of 5 ns in the NpT ensemble with only one ectoine molecule and 618 water molecules. A snapshot of the system with a central water molecule and 9 surrounding water molecules and a snapshot of bulk water with 11 wa-

ter molecules were considered for the DFT calculations. The DFT calculations have been carried out with the freely available quantum chemistry program ORCA 2.9.1[40,41]. The presence of zwitterionic ectoine instead of the neutral counterpart was validated by a previous publication[19]. We chose the gradient-corrected GGA BLYP functional[42,43] with dispersion corrections[44–46] for all molecules and both systems with the def2-TZVPP basis set[47] (system I: ectoine + 9 water molecules and system II: 11 water molecules) and performed a SCF geometry optimization. The corresponding geometry optimized snapshot for ectoine with nine water molecules is shown in Fig. 2. The presence of a strong hydrogen bond netwerk around the carboxylgroup of ectoine is evident. With regard to the experimental conditions in absence of bulk water, it can be assumed that the hydration shell around molecules of the ectoine powder closely resembles the snapshot, which justifies our approach. The Raman spectra have been calculated with the method described in Ref.[48].

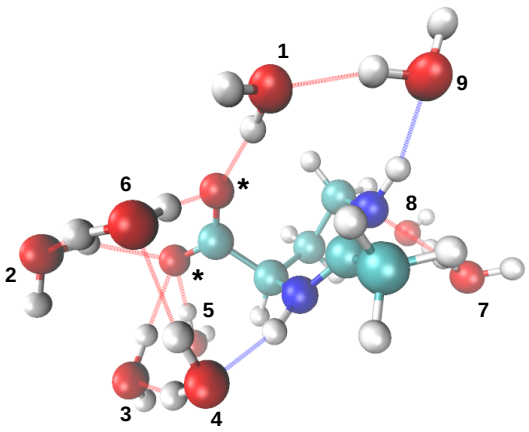

Figure 2: Snapshot of the geometry-optimized zwitterionic ectoine configuration with nine water molecules. Oxygen atoms of the COO^- group are marked with asterisks and form hydrogen bonds with the water molecules $1-5$. In addition, the water molecules $7-9$ form hydrogen bonds with the protonated nitrogen atoms of the pyrimidin ring. Red broken lines indicate hydrogen bonds with water molecules acting as donors whereas blue lines indicate hydrogen bonds with water molecules as acceptors. Hydrogen bonds are defined by a maximum acceptor-donor distance criterion of 0.35 nm and an angle of less than 35°.

Results

Properties of the first hydration shell around ectoine

Due to the high hygroscopicity of ectoine[19], it is possible to observe the hydration shell around single ectoine molecules by means of confocal Raman spectroscopy. The formation of the hydration shell around individual ectoine molecules is indicated by the appearance of water ν(O-H) modes. Thus, a stable water saturation state of ectoine can be observed in the upper spectrum of Fig. 3. The results indicate a preponderant ν(O-H) mode at 3445 cm^{-1}, a band at 3290 cm-1 and a range of less intense modes in close vicinity.

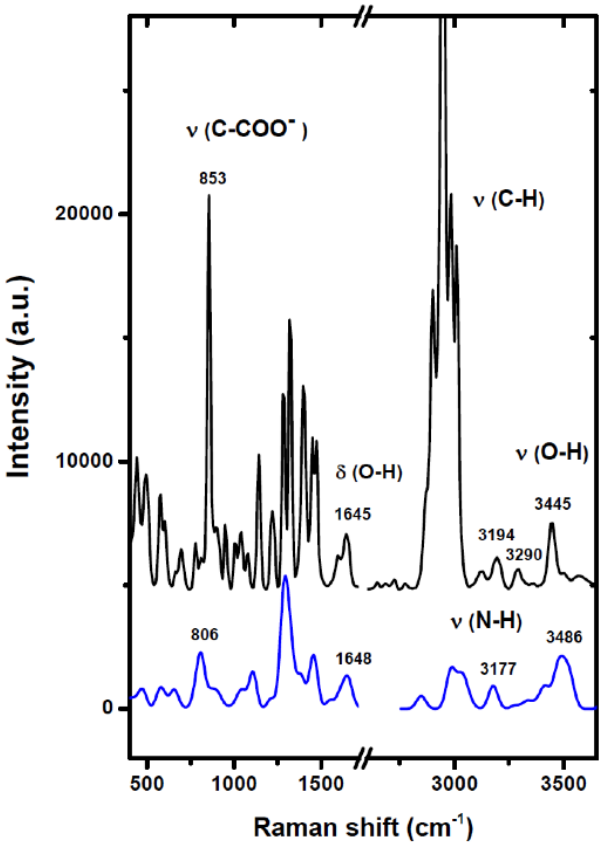

Figure 3: Confocal Raman spectrum of a saturated ectoine hydration shell (upper spectrum) due to an exposure of dry ectoine powder to water damp. DFT calculations of a Raman spectrum for a zwitterionic ectoine molecule surrounded by nine water molecules (lower spectrum).

The formation of the hydration shell is concurred with a phase-change like disappearance of the pair of the bands at 866 cm^{-1} and 780 cm^{-1} as given for the dry state. These bands are due to a Fermi-resonance between the ν(C-COO^-) mode at 853 cm^{-1} and a combination band involving COO^-(489 cm−1) and ring (359 cm−1) deformation modes. Upon the hydration the resonance is lifted and the strong band at 853 cm^{-1}characteristic for ectoine-water interactions appears. Noteworthy, the drying of ectoine at 95 °C temperatures exactly reverses this result such that the Fermi-resonance modes reappear and the ν(C-COO^-) mode vanishes. The experimentally observed bands at 3104 cm^{-1} and 3194 cm^{-1} were identified as intramolecular ectoine modes ν(N-H) by comparing the results between D_2O and H_2O. Due to the change in the reduced mass for D_2O, an identical behavior was observed under consideration of the frequency shift to the region around 2500 cm^{-1} (data not shown). The presence of the ν(N-H) mode can be also validated by the peak at 3177 cm^{-1} in the DFT calculations (lower spectrum shown in Fig. 3).

Further comparison with the calculated DFT Raman spectrum also reveals a significant peak at 3486 cm^{-1} corresponding to the experimentally observed intensity at 3445 cm^{-1}, which can be attributed to the strong binding of up to 5 H_2O molecules at the axially positioned COO^- group of ectoine (Fig. 2) in agreement with previous results of molecular dynamics simulations[19]. The presence of an axial carboxyl group conformation as calculated by the geometry optimization in the DFT calculations is also validated by crystal structure measurements and conformations obtained by NMR analysis and MP2 calculations of ectoine in solution[19,49]. Most importantly, the presence of the COO^- group strongly influences the surrounding water molecules[19]. Hence, a highly stable hydration shell around ectoine can be assumed. Most of the observed effects can be attributed to direct interactions between ectoine and water molecules, which become of specific importance at high molar ectoine concentrations. With regard to the 1.64 molar aqueous ectoine solution, our molecular dynamics (MD) simulation results reveal that nearly 80% of all water molecules are located within the first and the second hydration shell.

For the study of the hydration shell properties, the lifetime of hydrogen bonds can be calculated by the autocorrelation function[50]

$$C_{HB}(t) = \frac{\langle s_i(t_0) s_i(t) \rangle}{\langle s_i^2(t_0) \rangle} \tag{1}$$

with $s_i(t) = (0, 1)$ for a specific hydrogen bond i at time t where $s_i = 1$ denotes the existence of a hydrogen bond within a maximum donor-acceptor distance of 0.35 nm and an angle of 35°. The hydrogen bond forward lifetime τ_{HB} can then be calculated by

$$\langle \tau_{HB} \rangle = \int_0^\infty C_{HB}(t) dt \tag{2}$$

which is related to

$$\Delta F^\dagger \sim \log(\tau_{HB}/k_B T) \tag{3}$$

where $k_B T$ is the thermal energy and $\Delta F^\dagger$ can be interpreted as the activation energy to break an arbitrarily chosen hydrogen bond[17,51]. The corresponding MD results for a 1.64 molar ectoine solution reveal an average number of $N_{HB} = 6.1 \pm 0.1$ hydrogen bonds between ectoine and water molecules. The forward life time of the ectoine-water hydrogen bonds is given by $\langle \tau_{HB} \rangle \approx 10.6$ ps which is a factor of 2.7 higher than hydrogen bonds between water molecules in pure water with $\langle \tau_{HB} \rangle \approx 3.9$ ps. Interestingly, the hydrogen bonds between water molecules in aqueous ectoine solution also have a longer forward life with $\langle \tau_{HB} \rangle \approx 5.6$ ps when compared to pure water. These results indicate a strengthening of hydrogen bonds between water molecules in presence of ectoine which is in good agreement with previous findings[17]. The corresponding order in the activation energies $\Delta F^\dagger$ for the hydrogen bonds is therefore given by $\Delta F^\dagger$(ectoine-water)> $\Delta F^\dagger$(water(ectoine)-water(ectoine)) > $\Delta F^\dagger$(water(pure)-water(pure)).

Of particular importance in terms of the electrostatic properties of the solution are the molecular dipolar relaxation times and the values for the water dielectric constant. The

autocorrelation time for the dipolar orientation vector $\vec{\mu}$ can be calculated by

$$< \vec{\mu}(t)\vec{\mu}(t_0) > \sim \exp(-t/\tau)^{\beta}. \tag{4}$$

with the stretching exponent β[17,52]. The integration of Eqn. 4 yields

$$\langle \tau \rangle = \int_0^{\infty} dt \ \exp(-t/\tau)^{\beta} = \frac{\tau}{\beta}\Gamma\left(\frac{1}{\beta}\right) \tag{5}$$

where $\langle \tau \rangle$ is the mean relaxation time with the gamma function $\Gamma(...)$[17,19]. The resulting values for the dipolar relaxation times averaged over all water molecules are given by $\langle \tau \rangle \approx$ 8.9 ps (1.64 molar ectoine solution) and $\langle \tau \rangle \approx 4.6$ ps (pure water). The significant differences in the decay of the dipolar vector autocorrelation function (ACF) can be also seen in Fig. 4. Hence, with regard to the results discussed above, it can be clearly seen that the rotational behavior of water is slower in presence of ectoine, which corresponds to the fact that ectoine is a kosmotropic co-solute.

The strong influence on the dipolar relaxation times is also reflected by the value of the water dielectric constant which can be calculated by

$$\epsilon = 1 + \frac{4\pi}{3}\frac{\langle \vec{M}_{tot}^2 \rangle}{V k_B T} \tag{6}$$

where $\langle \vec{M}_{tot}^2 \rangle$ denotes the squared net total dipole moment of water molecules in the simulation box with volume V and thermal energy $k_B T$[53].

The corresponding results for the dielectric constant are given by $\epsilon = 53.5 \pm 0.1$ for water in presence of ectoine and $\epsilon = 70.5 \pm 0.2$ for pure water. Thus, the presence of ectoine leads to a significant decrease of the water dielectric constant. Furthermore, it has to be noted that the dielectric constant of the solution (ectoine and water) is given by $\epsilon = 89.7 \pm 0.6$. All values are summarized in Tab. 1.

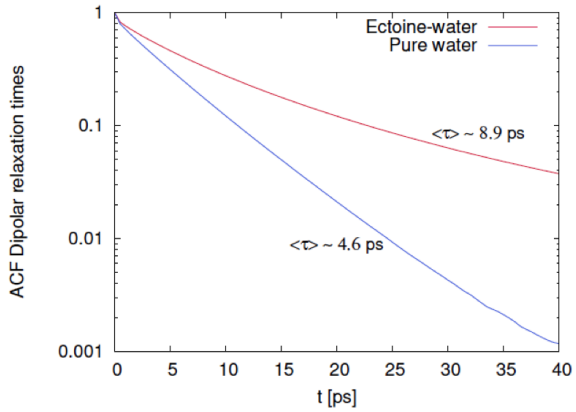

Figure 4: Autocorrelation function for the dipole orientation vector of water molecules in presence (blue line) and in absence of ectoine (red line).

Table 1: Simulation results for pure water and water in a 1.64 molar aqueous ectoine solution.

	Pure water	Water with ectoine ($c = 1.64$) mol/L
Forward life times $\langle \tau_{HB} \rangle$ [ps]	≈ 3.9	≈ 5.6
Dipolar relaxation times $\langle \tau \rangle$ [ps]	≈ 4.6	≈ 8.9
Water dielectric constant ϵ	70.5 ± 0.2	53.5 ± 0.1

Influence of ectoine on the binding behavior of protein G5P to DNA oligonucleotides

Amount of bound protein to DNA: Surface plasmon resonance data

With regard to the previous findings, which indicate a variation of the electrostatic properties of the solution in presence of the co-solute, it can be assumed that ectoine also has an influence on the binding of the protein G5P to highly charged immobilized single-stranded oligonucleotides (dT_{25}) in terms of an indirect mechanism. The G5P-DNA binding reaction is of fundamental importance in biology and biotechnology and is involved in a variety of important cellular processes such as DNA replication. We will discuss the binding of the gene-5-protein to the nucleotide strand in terms of surface plasmon resonance data. G5P is a small (87 amino acids with known sequence[54]), well-studied dimeric protein that binds

with two units to two separate single-stranded DNA (ssDNA) regions without significant sequence dependence. The resulting complex with ssDNA was previously examined by electron microscopy[55], circular dichroism[56] and Raman spectroscopy[57].

In Fig. 5, we present SPR data concerning the influence of ectoine on the binding of G5P molecules to immobilized single-stranded DNA (dT_{25}).

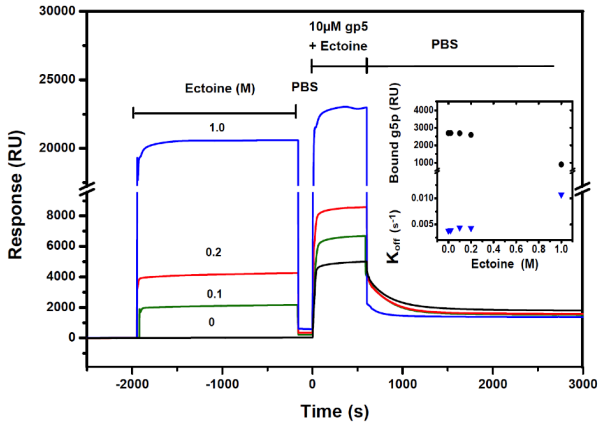

Figure 5: SPR data concerning the interaction of G5P with immobilized ssDNA (dT_{25}) in the absence and in the presence of ectoine. The surface was first exposed to ectoine alone in 1×PBS and then to ectoine with 10 μM G5P in 1×PBS solution. The sensogram for 0.01 molar ectoine concentration is omitted for reasons of clarity. The flow rate was 10 μl/min. Inset: The corresponding amount of bound G5P in RU units and the dissociation constant K_{off} of G5P-dT_{25}.

The sensogram without ectoine in solution demonstrates the high affinity of G5P for ssDNA. The amount of bound G5P corrected for the bulk contribution is determined as 2702 RU (green line in Fig. 5), corresponding to an average number of 3.5 G5P molecules which are directly interacting with each immobilized dT_{25} oligonucleotide. This value can be compared to the expected one G5P molecule per four nucleotides which has been reported in Ref. 58 for mobile ssDNA in solution. The presence of a 1 molar ectoine solution strongly reduces the amount of bound G5P to about one third of the value obtained in the absence of ectoine. Interestingly, for concentrations below 0.2 mol/L, ectoine induces only a small decrease (about 10%) in the number of G5P-DNA complexes as can be seen in the inset of Fig. 5. Only a small change in the stability of the protein-DNA complex in this concentration

range is observed. This is also reflected by comparable values of the dissociation constant K_{off} for these concentrations as calculated by simple exponential decay kinetics. Indeed, the dissociation constant increases by a factor of 2.7 for a 1 molar ectoine solution when compared to pure water which indicate a destabilization of the G5P-DNA complex. Thus, it can be safely assumed that the interaction mechanism between ectoine and biomolecules strongly depends on the concentration in agreement with previous results for other co-solutes[6] as well as ectoine[17,22,23,59].

Finally, we studied the effects of ectoine on the G5P secondary structure by Raman spectroscopy. Fig. 6 presents the Raman spectra of G5P protein (12.6 mg/ml in 2×PBS) , ectoine (1 mol/L in water) and pure water which allows us to distinguish between the different contributions. As a prerequisite, the ectoine contribution was subtracted from the G5P data by using its characteristic band at 1141 cm^{-1}. The validity of this procedure was also checked by using other bands of ectoine, *e. g.*, ν(C-COO^-) at 850 cm^{-1} and δ(C-COO^-) at 595 cm^{-1}.

In Fig. 7 we present the final amide I band region for G5P in absence and in presence of a 1 molar aqueous ectoine solution after the subtraction of the solvent and the co-solute contributions as described above.

The band fitting procedure, as described in the previous section, revealed two major components at 1670 cm^{-1} and 1654 cm^{-1} and two shoulder bands at 1687 cm^{-1} and 1635 cm^{-1}. The band at 1670 cm^{-1} is a marker band for β-sheet conformation and the band at 1654 cm^{-1} is characteristic for alpha-helical peptide bonds[29–32]. The differences in the peaks in terms of the absolute values for a system with ectoine and without ectoine are significant. For G5P in absence of ectoine in solution, the fit indicates that the protein's secondary structure is composed of 59% β-sheets and 25% α-helices. This finding is in very good agreement with the results of a previous Raman spectroscopy study of G5P[57] where the corresponding values were 52% β-sheets and 19% α-helices, respectively.

However, a significant change can be observed in presence of ectoine (Fig. 7, upper spectrum).

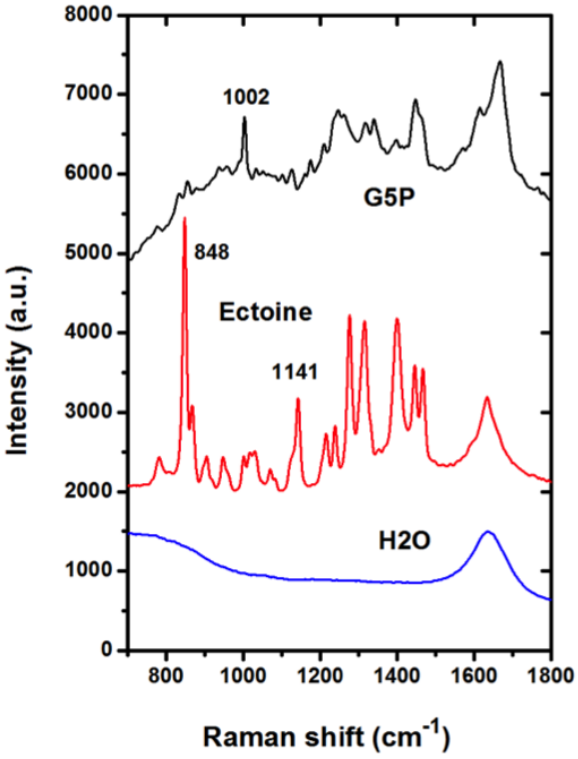

Figure 6: Raman spectra of G5P protein (12.6 mg/ml in 2×PBS) after subtraction of the solvent contribution, aqueous ectoine (1 mol/L in water) after subtraction of the water contribution and pure water.

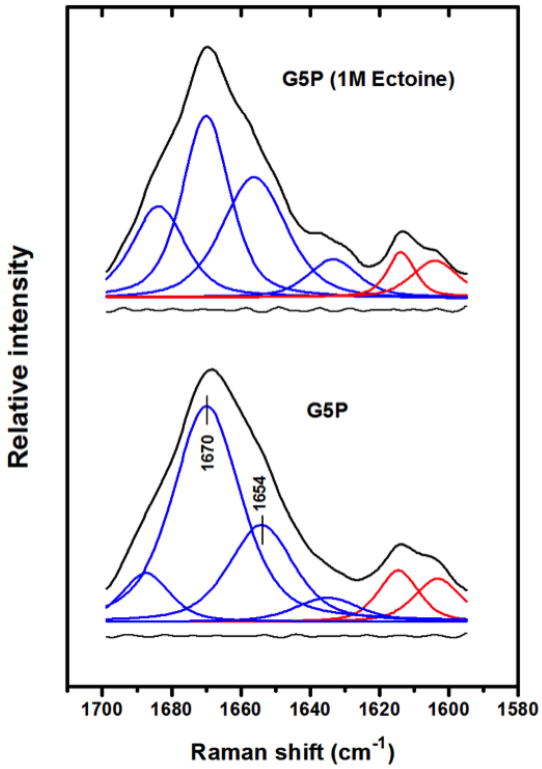

Figure 7: Raman spectra in the amide I region for the G5P protein in the absence (lower spectrum) and in the presence of a 1 molar ectoine solution (upper spectrum). The spectra were processed and fitted according to the procedure described in the experimental part. The residual of the fit is also shown (thin line below the spectra). The β-sheet and α-helix contribution are observed at 1670 cm^{-1} and 1654 cm^{-1}, respectively.

The contribution related to β-sheets thereby decreases to about 39%, and the contribution from α-helix elements increases to 33%. Thus, at 1 molar ectoine concentration, there is quite a significant change in the protein conformation that we tentatively suggest to be responsible for the decay of the protein's bioactivity as it was also found for the dissociation constant K_{off} (Fig. 5). All results are summarized in Tab. 2 and shown in Fig. 8.

Table 2: Percentages of secondary structure elements of G5P determined by curve fitting of the amide I bands in absence of ectoine (G5P) and in presence of a 1 molar aqueous ectoine solution (G5P+Ectoine).

Structure element	Position [cm^{-1}]	Percentage [%]
G5P		
β-turn	1687	10
β-sheet	1670	59
α-helix	1654	25
undefined	1635	6
G5P+Ectoine		
β-turn	1684	20
β-sheet	1670	39
α-helix	1656	33
undefined	1633	8

Discussion and Conclusion

We have studied the influence of ectoine on its local hydration shell and on the binding of gene-5-proteins to oligonucleotide strands. Our results reveal a strong change in the electrostatic properties of the solution, which might have important consequences for the binding of G5P to the nucleotides. Our SPR data indicate a strong variation of the G5P-DNA dissociation constant in presence of high molar ectoine concentrations. In addition, a significant change of the protein conformation in terms of secondary structure elements in presence of ectoine has been found.

Two explanations can be suggested, one from the DNA side and the other from the protein

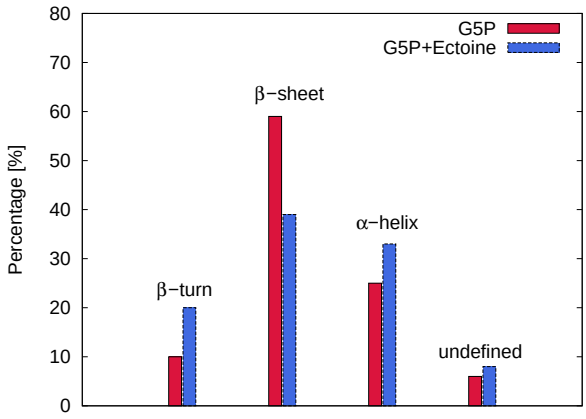

Figure 8: Percentages of secondary structure elements of G5P determined by curve fitting of the amide I bands in absence of ectoine (G5P, red bars) and in presence of a 1 molar aqueous ectoine solution (G5P+Ectoine, blue bars).

side. It is known from a ^{23}Na NMR study[60] that zwitterionic compatible solutes decrease the amount of sodium ions in the vicinity of DNA, an effect which inevitably exerts an influence on DNA bioactivity. This explanation is in agreement with the observed residual value of 538 RU after exposure of ssDNA to 1 molar ectoine solution without G5P followed by washing (left part of the sensogram in Fig. 5). The response value implies an average number of about two ectoine molecules which are interacting, presumable electrostatically in addition to dispersion interactions, with a single nucleotide of the immobilized ssDNA. This effect becomes also reasonable with regard to the zwitterionic and bulky properties of ectoine and due to the result of a previous study[19], where it has been reported that ectoine molecules mainly interact electrostatically with DPPC lipid bilayers.

In addition, it has to be noted that the presence of ectoine strongly changes the electrostatic properties of the solution as it has been validated by the Molecular Dynamics simulation results. The importance of electrostatic interaction for proteins has also been recognized previously[61,62]. This might have some consequences for the binding of the protein to DNA. In fact, structural studies of G5P[58,63] indicated the presence of highly charged regions which are of specific importance for the binding to DNA. Recent results also indicated a strong decrease of the dielectric constant of water in confined geometries, at interfaces and in

electrolyte solutions[? ? ?] . Therefore, it can be assumed that all contributions in addition to the presence of ectoine might have important consequences for the binding behavior. Furthermore, also the changed conformations of G5P might affect the binding properties. Moreover, it can be assumed that ectoine molecules cover the solvent accessible surface area of the DNA in a distance of around 0.5 nm, as it has been found for DPPC lipid bilayers[19]. This behavior might also drastically diminish the free surface area for the interacting protein. Nevertheless, based on our findings, we assume that the change of the solution properties as induced by ectoine plays the major role in the G5P-DNA binding behavior. The detailed reasons will be studied in the future. We greatly acknowledge the financial support of the Deutsche Forschungsgemeinschaft (DFG) through the projects (STU 245/4-1) and (BI 536/3-1) and through the cluster of excellence initiative Simulation Technology (EXC 310) and the SFB 716. We are also thankful for the helpful discussions with Pavel Jungwirth and Nico van der Vegt.

References

(1) Yancey, P. H. Organic osmolytes as compatible, metabolic and counteracting cytoprotectants in high osmolarity and other stresses. *Journal of Experimental Biology* **2005**, *208*, 2819–2830.

(2) Oren, A. Microbial life at high salt concentrations: phylogenetic and metabolic diversity. *Saline Systems* **2008**, *4*, 2.

(3) Roberts, M. F. Organic compatible solutes of halotolerant and halophilic microorganisms. *Saline Systems* **2006**, *1*, 1–30.

(4) Kunte, H. J. Osmoregulation in bacteria: compatible solute accumulation and osmosensing. *Environ. Chem.* **2006**, *3*, 94–99.

(5) Lentzen, G.; Schwarz, T. Extremolytes: natural compounds from extremophiles for versatile applications. *Appl. Microbiol. Biotechnol.* **2006**, *72*, 623–634.

(6) Canchi, D. R.; García, A. E. Cosolvent effects on protein stability. *Annual review of physical chemistry* **2013**, *64*, 273–293.

(7) Zhang, Y.; Cremer, P. S. Chemistry of Hofmeister anions and osmolytes. *Annual review of physical chemistry* **2010**, *61*, 63–83.

(8) Schwibbert, K.; Marin-Sanguino, A.; Bagyan, I.; Heidrich, G.; Lentzen, G.; Seitz, H.; Rampp, M.; Schuster, S. C.; Klenk, H.-P.; Pfeiffer, F.; Oesterhelt, D.; Kunte, H. J. A blueprint of ectoine metabolism from the genome of the industrial producer Halomonas elongata DSM 2581^T. *Environmental Microbiology* **2011**, *13*, 1973–1994.

(9) Kunte, H. J.; Lentzen, G.; Galinski, E. A. Industrial production of the cell protectant ectoine: protection mechanisms, processes, and products. *Curr. Biotech.* **2014**, *3*, 10–25.

(10) Lee, C. J.; Timasheff, S. N. The stabilization of proteins by sucrose. *J. Biol. Chem.* **1981**, *256*, 2969–2978.

(11) Timasheff, S. N. Protein hydration, thermodynamic binding, and preferential hydration. *Biochemistry* **2002**, *41*, 13473–13482.

(12) Street, T.; Bolen, D.; Rose, G. A molecular mechanism for osmolyte-induced protein stability. *PNAS* **2006**, *103*, 17064–17065.

(13) Bolen, D. W.; Rose, G. D. Structure and energetic of the hydrogen-bonded backbone in protein folding. *Annu. Rev. Biochem.* **2008**, *77*, 339–362.

(14) Collins, K. D. Charge density-dependent strength of hydration and biological structure. *Biophysical Journal* **1997**, *72*, 65–76.

(15) Collins, K. D. Ions from the Hofmeister series and osmolytes: effects on proteins in solution and in the crystallization process. *Methods* **2004**, *34*, 300–311.

(16) Collins, K. D.; Neilson, G. W.; Enderby, J. E. Ions in water: characterizing the forces that control chemical processes and biological structure. *Biophysical chemistry* **2007**, *128*, 95–104.

(17) Smiatek, J. Osmolyte effects: impact on the aqueous solution around charged and neutral spheres. *J. Phys. Chem. B* **2014**, *118*, 771–82.

(18) Lesch, V.; Heuer, A.; Tatsis, V. A.; Holm, C.; Smiatek, J. Peptides in presence of aqueous ionic liquids: Tunable co-solutes as denaturants or protectants? *Phys. Chem. Chem. Phys.* **2015**, DOI:10.1039/c5cp03838c.

(19) Smiatek, J.; Harishchandra, R. K.; Rubner, O.; Galla, H.-J.; Heuer, A. Properties of compatible solutes in aqueous solution. *Biophysical chemistry* **2012**, *160*, 62–68.

(20) Narayanan Krishnamoorthy, A.; Holm, C.; Smiatek, J. Local Water Dynamics Around Antifreeze Protein Residues in Presence of Osmolytes-The Importance of Hydroxyl and Disaccharide Groups. *The Journal of Physical Chemistry B* **2014**, *118*, 11613–11621.

(21) Harishchandra, R. K.; Wulff, S.; Lentzen, G.; Neuhaus, T.; Galla, H.-J. The effect of compatible solute ectoines on the structural organization of lipid monolayer and bilayer membranes. *Biophysical chemistry* **2010**, *150*, 37–46.

(22) Smiatek, J.; Harishchandra, R. K.; Galla, H.-J.; Heuer, A. Low concentrated hydroxyectoine solutions in presence of DPPC lipid bilayers: a computer simulation study. *Biophysical chemistry* **2013**, *180*, 102–109.

(23) Kurz, M. Compatible solute influence on nucleic acids: Many questions but few answers. *Saline Systems* **2008**, *4*, 6–20.

(24) Schnooe, M.; Voss, P.; Cullen, P.; Boking, T.; Galla, H.-J.; Galinski, E. A.; Lorkowski, S. Charactersation of the synthetic compatible solute homoectoine as a potent PCR enhancer. *Biochem. Biophys. Res. Comm.* **2004**, *322*, 867–872.

(25) Solomun, T.; Sturm, H.; Wellhausen, R.; Seitz, H. Interaction of a single-stranded DNA-binding protein g5p with DNA oligonucleotides immobilised on a gold surface. *Chemical Physics Letters* **2012**, *533*, 92–94.

(26) Lee, S.-K.; Maye, M. M.; Zhang, Y.-B.; Gang, O.; van der Lelie, D. Controllable g5p-Protein-Directed Aggregation of ssDNA- Gold Nanoparticles. *Langmuir* **2008**, *25*, 657–660.

(27) Peterson, A.; Heaton, R.; RM., G. The effect of surface probe density on DNA hybridization. *Nucleic Acids Research* **2001**, *29*, 5163–5168.

(28) Schoch, R. L.; Lim, R. Y. Non-interacting molecules as innate structural probes in surface plasmon resonance. *Langmuir* **2013**, *29*, 4068–4076.

(29) Alix, A.; Pedanou, G.; Berjot, M. Fast determination of the quantitative secondary structure of proteins by using some parameters of the Raman amide I band. *Journal of Molecular Structure* **1988**, *174*, 159–164.

(30) Carey, P. *Biochemical applications of Raman and resonance Raman spectroscopes*; Elsevier, 2012.

(31) Overman, S. A.; Thomas, G. J. Amide modes of the α-helix: Raman spectroscopy of filamentous virus fd containing peptide 13C and 2H labels in coat protein subunits. *Biochemistry* **1998**, *37*, 5654–5665.

(32) Dong, J.; Wan, Z.-L.; Chu, Y.-C.; Nakagawa, S. N.; Katsoyannis, P. G.; Weiss, M. A.; Carey, P. R. Isotope-edited Raman spectroscopy of proteins: a general strategy to probe individual peptide bonds with application to insulin. *Journal of the American Chemical Society* **2001**, *123*, 7919–7920.

(33) Spoel, D. V. D.; Lindahl, E.; Hess, B.; Groenhof, G.; Mark, A. E.; Berendsen, H. J. C.

GROMACS: Fast, flexible, and free. *Journal of Computational Chemistry* **2005**, *26*, 1701–1718.

(34) Pronk, S.; Páll, S.; Schulz, R.; Larsson, P.; Bjelkmar, P.; Apostolov, R.; Shirts, M. R.; Smith, J. C.; Kasson, P. M.; van der Spoel, D.; Hess, B.; Lindahl, E. GROMACS 4.5: a high-throughput and highly parallel open source molecular simulation toolkit. *Bioinformatics* **2013**, *29*, 845–854.

(35) Berendsen, H. J. C.; Grigera, J. R.; Straatsma, T. P. The missing term in effective pair potentials. *J. Phys. Chem.* **1987**, *91*, 6269–6271.

(36) Darden, T.; York, D.; Pedersen, L. Particle mesh Ewald: An N log (N) method for Ewald sums in large systems. *The Journal of chemical physics* **1993**, *98*, 10089–10092.

(37) Evans, D. J.; Holian, B. L. The NoseHoover thermostat. *J. Chem. Phys.* **1985**, *83*, 4069–4074.

(38) Parrinello, M.; Rahman, A. Polymorphic transitions in single crystals: A new molecular dynamics method. *J. Appl. Phys.* **1981**, *52*, 7182–7190.

(39) Hess, B.; Bekker, H.; Berendsen, H. J. C.; Fraaije, J. G. E. M. {LINCS}: {A} linear constraint solver for molecular simulations. *J. Comput. Chem.* **1997**, *18*, 1463–1472.

(40) Neese, F.; *et. al.*, Orca. *An ab Initio, Density Functional and Semiempirical Program Package version* **2009**, *2*.

(41) Neese, F. The ORCA program system. *WIRes: Comp. Mol. Sci.* **2012**, *2*, 73–78.

(42) Becke, A. D. Density-functional thermochemistry. III. The role of exact exchange. *J. Chem. Phys.* **1993**, *98*, 5648–5652.

(43) Lee, C.; Yang, W.; Parr, R. G. Development of the Colle-Salvetti correlation-energy formula into a functional of the electron density. *Phys. Rev. B* **1988**, *37*, 785.

(44) Grimme, S. Accurate description of van der Waals complexes by density functional theory including empirical corrections. *J. Comp. Chem.* **2004**, *25*, 1463–1473.

(45) Grimme, S. Semiempirical GGA-type density functional constructed with a long-range dispersion correction. *J. Comp. Chem.* **2006**, *27*, 1787–1799.

(46) Grimme, S.; Antony, J.; Ehrlich, S.; Krieg, H. A consistent and accurate ab initio parametrization of density functional dispersion correction (DFT-D) for the 94 elements H-Pu. *J. Chem. Phys.* **2010**, *132*, 154104.

(47) Weigend, F.; Ahlrichs, R. Balanced basis sets of split valence, triple zeta valence and quadruple zeta valence quality for H to Rn: design and assessment of accuracy. *Phys. Chem. Chem. Phys.* **2005**, *7*, 3297–3305.

(48) Petrenko, T.; Neese, F. Analysis and prediction of absorption band shapes, fluorescence band shapes, resonance Raman intensities, and excitation profiles using the time-dependent theory of electronic spectroscopy. *J. Chem. Phys.* **2007**, *127*, 164319.

(49) Schuh, W.; Puff, H.; Galinski, E. A.; Trüper, H. G. Die Kristallstruktur des Ectoin, einer neuen osmoregulatorisch wirksamen Aminosäure/The Crystal Structure of Ectoine, a Novel Amino Acid of Potential Osmoregulatory Function. *Zeitschrift für Naturforschung C* **1985**, *40*, 780–784.

(50) Luzar, A.; Chandler, D. Hydrogen-bond kinetics in liquid water. *Nature* **1996**, *379*, 55–57.

(51) van der Spoel, D.; van Maaren, P. J.; Larsson, P.; Timneanu, N. Thermodynamics of hydrogen bonding in hydrophilic and hydrophobic media. *The Journal of Physical Chemistry B* **2006**, *110*, 4393–4398.

(52) Kumar, P.; Franzese, G.; Buldyrev, S. V.; Stanley, H. E. Molecular dynamics study of orientational cooperativity in water. *Physical Review E* **2006**, *73*, 041505.

(53) Neumann, M. Dipole moment fluctuation formulas in computer simulations of polar systems. *Mol. Phys.* **1983**, *50*, 841–858.

(54) Cuypers, T.; van der Ouderaa, F. J.; de Jong, W. W. The amino acid sequence of gene 5 protein of bacteriophage M 13. *Biochemical and biophysical research communications* **1974**, *59*, 557–563.

(55) Olah, G. A.; Gray, D. M.; Gray, C. W.; Kergil, D. L.; Sosnick, T. R.; Mark, B. L.; Vaughan, M. R.; Trewhella, J. Structures of fd Gene 5 Protein· Nucleic Acid Complexes: A Combined Solution Scattering and Electron Microscopy Study. *Journal of molecular biology* **1995**, *249*, 576–594.

(56) Scheerhagen, M.; Bokma, J.; Vlaanderen, C.; Blok, J.; Van Grondelle, R. A specific model for the conformation of single-stranded polynucleotides in complex with the helix-destabilizing protein GP32 of bacteriophage T4. *Biopolymers* **1986**, *25*, 1419–1448.

(57) Otlo, C.; De Mul, F.; Hannsen, B.; Greve, J. A Raman scattering study of the helix-destabilizing gene-5 protein with adenine-containing nucleotides. *Nucleic acids research* **1987**, *15*, 7605–7625.

(58) Guan, Y.; Zhang, H.; Wang, A. H.-J. Electrostatic potential distribution of the gene V protein from Ff phage facilitates cooperative DNA binding: A model of the GVP-ssDNA complex. *Protein Science* **1995**, *4*, 187–197.

(59) Ablinger, E.; Hellweger, M.; Leitgeb, S.; Zimmer, A. Evaluating the effects of buffer conditions and extremolytes on thermostability of granulocyte colony-stimulating factor using high-throughput screening combined with design of experiments. *International journal of pharmaceutics* **2012**, *436*, 744–752.

(60) Flock, S.; Labarbe, R.; Houssier, C. ^{23}Na NMR study of the effect of organic osmolytes on DNA counterion atmosphere. *Biophysical journal* **1996**, *71*, 1519.

(61) Perutz, M. Electrostatic effects in proteins. *Science* **1978**, *201*, 1187–1191.

(62) Warshel, A.; Russell, S. T. Calculations of electrostatic interactions in biological systems and in solutions. *Quarterly reviews of biophysics* **1984**, *17*, 283–422.

(63) McPherson, A.; Jurnak, F.; Wang, A.; Kolpak, F.; Rich, A.; Molineux, I.; Fitzgerald, P. The structure of a DNA unwinding protein and its complexes with oligodeoxynucleotides by x-ray diffraction. *Biophysical journal* **1980**, *32*, 155.